SCATTERING CHARACTERISTICS OF A PARTIALLY DEBONDED COMPLIANT INCLUSION-MATRIX INTERPHASE

M. Kitahara

Tokai University
Shimizu, Shizuoka 424, Japan

K. Nakagawa

Total System Institute
Shinjuku, Tokyo 162, Japan

J. D. Achenbach

Center for Quality Engineering
and Failure Prevention
Northwestern University
Evanston, IL 60208

INTRODUCTION

Scattering characteristics have been calculated for a spherical inclusion with partially debonded interphase conditions. Three scattering characteristics of the scattered field have been selected for investigation: 1) the frequency response at a fixed point, 2) the scattered field at a fixed frequency along an observation line, and 3) the radiation pattern. The compliant interphase between the inclusion and the surrounding elastic matrix has been modeled by a layer of distributed springs which offers resistance to relative displacements in the two tangent and the normal directions. Two basic assumptions are made for the spring model of the interphase: 1) The springs are linear, and 2) The interphase is very thin so that the effect of inertia of the interphase can be neglected. These assumptions are acceptable in the low frequency range. The partial debonding of the interphase is modeled by setting the spring constants (defined per unit area) equal to zero along part of the interphase.

The method of solution is based on the 3D elastodynamic boundary integral equation method. The treatment of the interphase and the solution strategy have been discussed in detail in our previous paper[1]; so we omit the details here. The spring model has been reviewed in some recent articles by Baik and Thompson[2], and Martin[3].

SUMMARY OF THE FORMULATION

The integral representation for the exterior displacement field can be expressed as

$$u_i(\mathbf{x}) = \int_S U_{ij}(\mathbf{x},\mathbf{y})t_j(\mathbf{y})dS_y - \int_S T_{ij}(\mathbf{x},\mathbf{y})u_j(\mathbf{y})dS_y + u_i^I(\mathbf{x}), \qquad \mathbf{x}\in D, \tag{1}$$

where S is the interphase boundary at the matrix side and U_{ij} is the fundamental solution for 3D time-harmonic elastodynamics. The boundary integral equation for the exterior matrix may subsequently be obtained as

Review of Progress in Quantitative Nondestructive Evaluation, Vol. 9
Edited by D.O. Thompson and D.E. Chimenti
Plenum Press, New York, 1990

$$C_{ij}(x)u_j(x) = \int_S U_{ij}(x,y)t_j(y)dS_y - \int_S T_{ij}(x,y)u_j(y)dS_y + u_i^I(x), \quad x \in S. \tag{2}$$

The boundary integral equation for the inclusion is of the form

$$\bar{C}_{ij}(x)\bar{u}_j(x) = \int_{\bar{S}} \bar{U}_{ij}(x,y)\bar{t}_j(y)dS_y - \int_{\bar{S}} \bar{T}_{ij}(x,y)\bar{u}_j(y)dS_y, \qquad x \in \bar{S}, \tag{3}$$

where $\bar{S}$ is the interphase boundary at the inclusion side.

The discretization process, the equations for the interphase, and the interaction conditions are all the same as in the previous paper[1]. As shown in Ref.[1], the final matrix form of the equations may be written as

$$\begin{pmatrix} \bar{\mathbf{K}}+\mathbf{S} & -\mathbf{S} \\ -\mathbf{S} & \mathbf{K}+\mathbf{S} \end{pmatrix} \begin{pmatrix} \bar{\mathbf{u}} \\ \mathbf{u} \end{pmatrix} = \begin{pmatrix} \mathbf{0} \\ \mathbf{A}\mathbf{G}^{-1}\mathbf{u}^I \end{pmatrix} \tag{4}$$

where $\bar{\mathbf{K}}$ and $\mathbf{K}$ are double layer matrices, $\mathbf{G}$ is a simple layer matrix, and $\mathbf{A}$ is the area matrix. The interphase conditions are characterized by the spring matrix $\mathbf{S}$:

$$\mathbf{S} = \begin{Bmatrix} \mathbf{R}_1 & & & \mathbf{0} \\ & \mathbf{R}_2 & & \\ & & \ddots & \\ & & & \mathbf{R}_\alpha \\ & & & & \ddots \\ \mathbf{0} & & & & & \mathbf{R}_M \end{Bmatrix}, \tag{5}$$

where M is the total number of the elements and $\mathbf{R}_\alpha$ has the following form:

$$\mathbf{R}_\alpha = \begin{pmatrix} R_{1\alpha}A_\alpha & 0 & 0 \\ 0 & R_{2\alpha}A_\alpha & 0 \\ 0 & 0 & R_{3\alpha}A_\alpha \end{pmatrix}, \text{ (no sum on } \alpha) \tag{6}$$

where $R_{1\alpha}$, $R_{2\alpha}$, and $R_{3\alpha}$ are spring constants per unit area in the x_1, x_2, and x_3 directions, respectively, and A_α is the area of the α-th element.

NUMERICAL MODEL

We consider a spherical inclusion with radius d, which is referred to spherical coordinates (r, θ, ϕ) as shown in Fig.1. The incident wave is a plane longitudinal wave traveling along the x_3 direction: $\mathbf{u}^I=\exp(ik_Lx_3)\mathbf{e}_3$. The material properties of the inclusion are defined by $\bar{c}_L/c_L=1/\sqrt{2}$, $\bar{\nu}=\nu=1/4$, $\bar{\rho}/\rho=1$, which imply that the inclusion is somewhat softer than the matrix material

The spring stiffnesses ($R_{r\alpha}$, $R_{\theta\alpha}$, $R_{\phi\alpha}$) per unit area are nondimensionalized to the forms $R_{r\alpha}/R_0$, $R_{\theta\alpha}/R_0$, and $R_{\phi\alpha}/R_0$, where $R_0= \rho c_L^2/d$, and for the present calculation we set $SP_\alpha \equiv R_{r\alpha}/R_0=R_{\theta\alpha}/R_0=R_{\phi\alpha}/R_0$. Note that SP_α may change from element to element. For an element on a traction free crack face, we set $SP_\alpha=0$.

EXAMPLES

Figure 2 shows the general trend for the frequency dependence of the amplitude of the back scattered field, when the insonified side of the inclusion is crack surface(SP=0). The spring

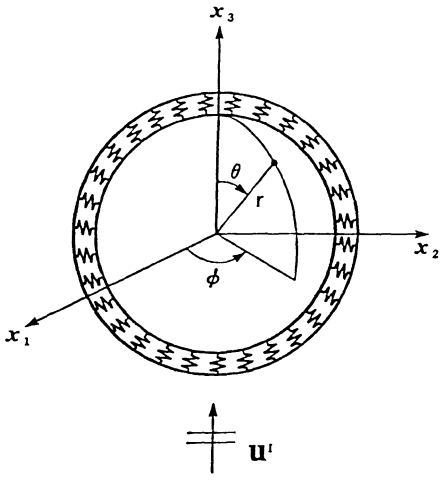

Fig.1 Spherical inclusion with radius d.

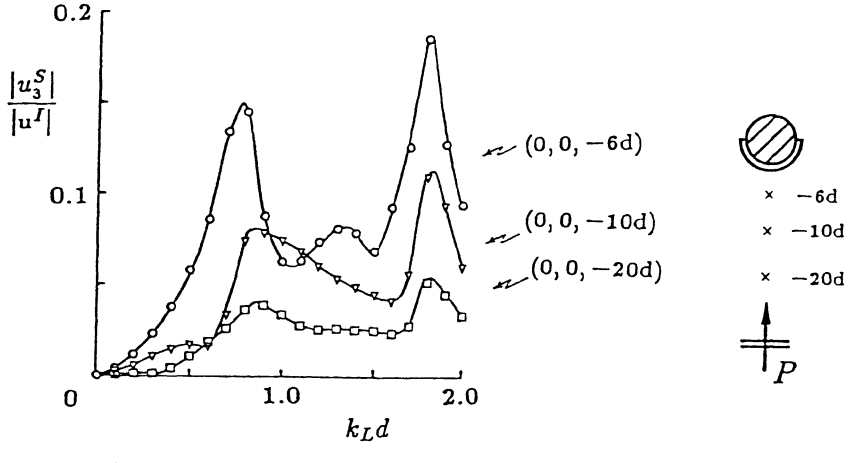

Fig.2 Scattered field amplitudes $|u_3^S|/|u^I|$ vs. wave number $k_L d$.

constants over the intact shadow side were chosen as SP=100. The three curves depict the back scattered fields at three points: x_3=-6d, -10d, and -20d. In the near field(x_3=-6d), rather sharp peaks can be observed compared with the results for the perfectly bonded inclusion[4].

The top curves of Fig.3 show the absolute value, and the real and imaginary parts of u_3^S at x_3=-2d ~ -40d for k_Ld=1.0, and for the case of a crack over the insonified side of the spherical inclusion. The spring constants over shadow side are SP=5. For comparison, back scattered results for three different types of inclusions of interphase conditions are also shown in this figure. They are perfect bonding over the surface, a cavity, and a crack at the shadow side. The thick arrows are attached to indicate points of the same phase. We can see that the back scattered amplitude for the case of perfect bonding is very small as compared with the

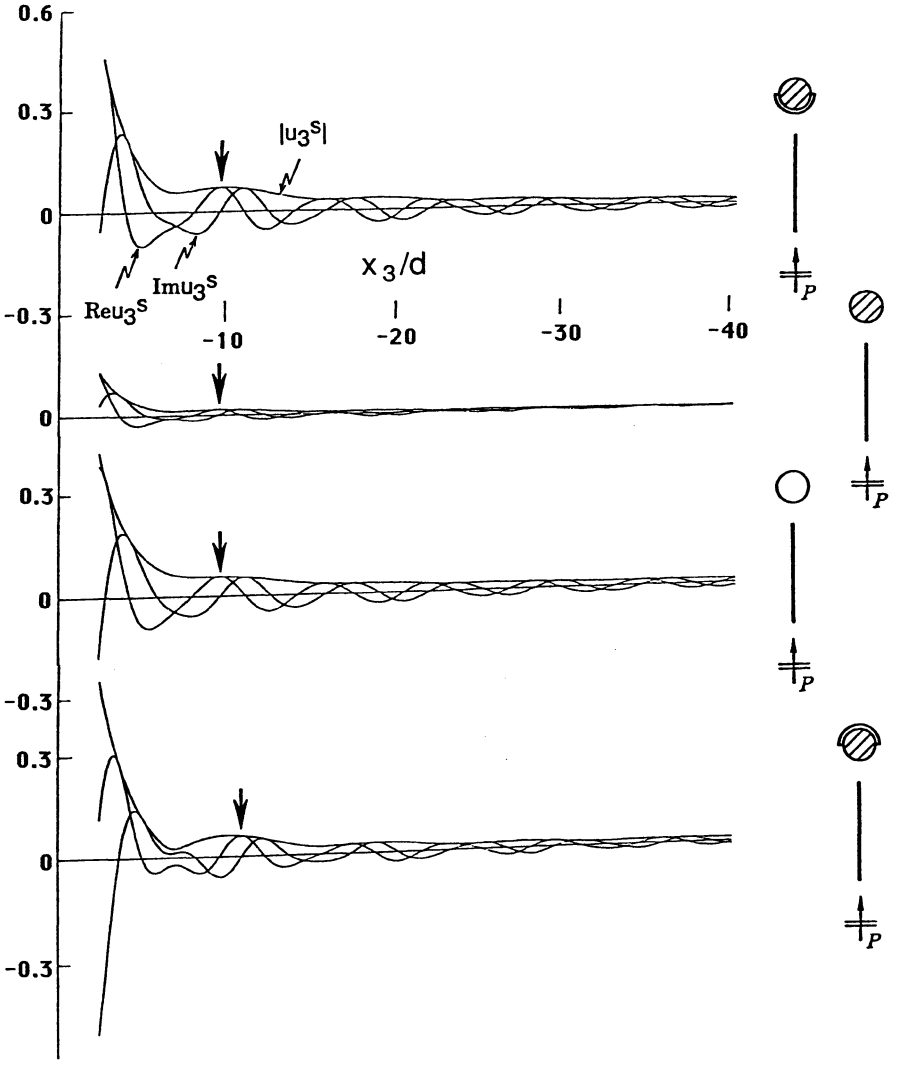

Fig.3 Comparison of back scattered fields at k_Ld=1.0.

other cases. For the crack at the shadow side, the phase is shifted about by $\pi/4$ wave length. Figure 4 shows the forward scattered fields. The arrangement of the figures is the same as for Fig.3. Figure 5 shows the laterally scattered fields along the x_1-axis. For perfect bonding the component $|u_3^s|$ of the laterally scattered field is almost zero except for the vicinity of the inclusion. The laterally scattered field amplitudes for the cracked interphase, shown at the top and the bottom of Fig.5, are larger than for the case of a cavity. This may be due to tip diffraction by the interphase crack.

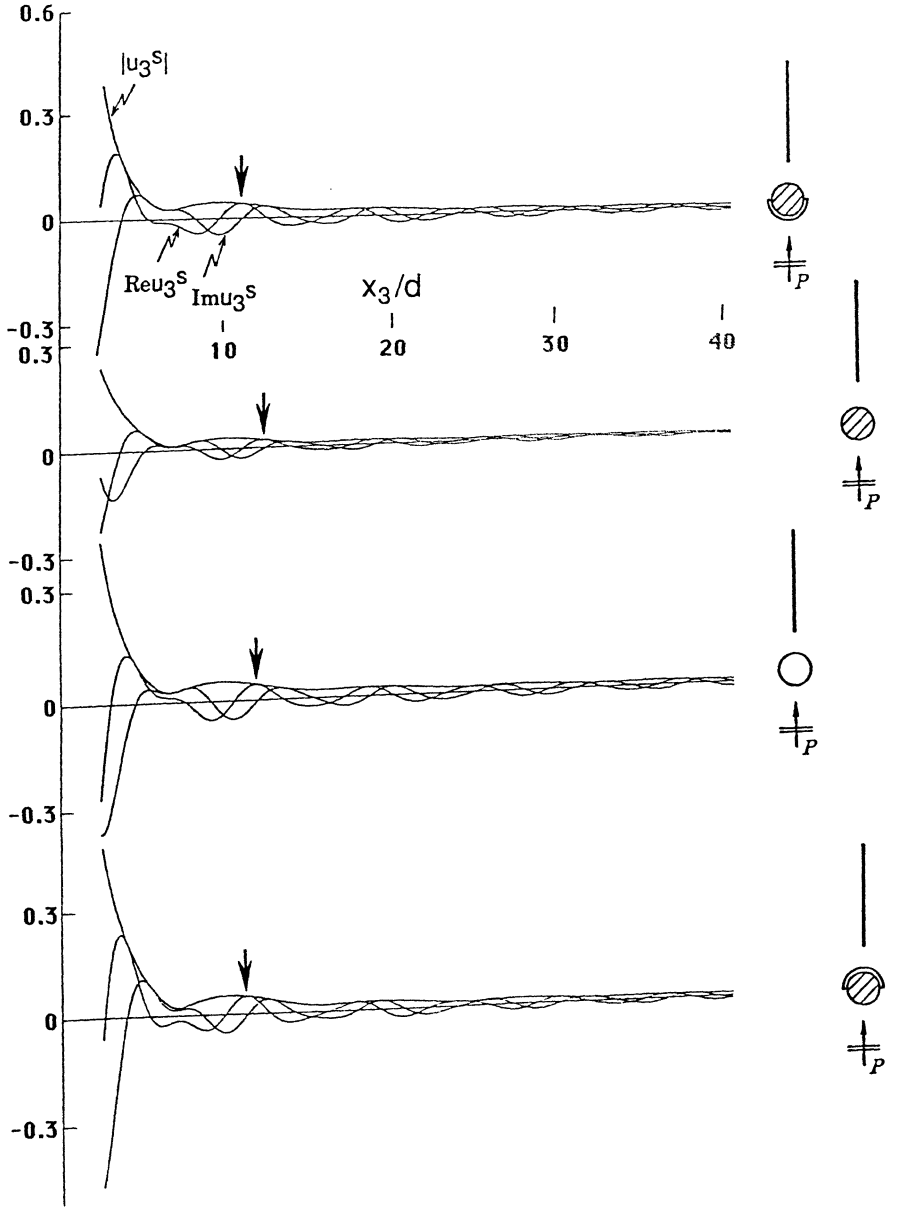

Fig.4 Comparison of forward scattered fields at $k_L d=1.0$.

Radiation patterns for three types of interphase conditions, namely, the cases of the crack at the insonified side, perfect bonding and the cavity are shown in Figs. 6, 7 and 8, respectively. These radiation patterns were calculated based on the scattered field

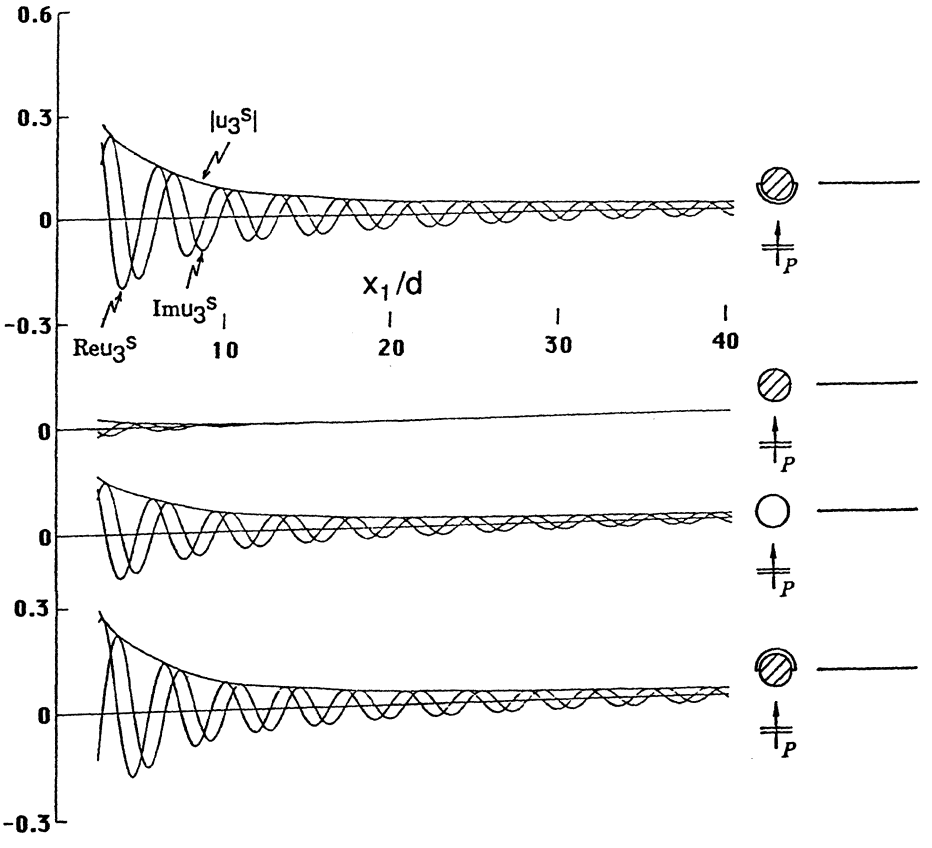

Fig.5 Comparison of laterally scattered fields at $k_L d=1.0$.

representation in Eq.(1). The radius of the field point x was chosen as $r/d = 50$. In these figures, the left hand sides are the absolute values and the right hand sides are the real and the imaginary parts of the scattered fields. The values are normalized by the maximum value for each figure. Only the shape of the pattern has meaning in this case. The absolute values $|u_r|$ of the radial components (upper left corner for each figure) are generally in the shape of egg. On the other hand, the absolute values $|u_\theta|$ of the polar components (lower left corner) have different patterns, such as two leaves, four leaves, and butterfly shaped, respectively, for the case of the half crack, perfect bonding, and the cavity. It appears that at some distance from the scatterer the polar component u_θ is sensitive to the interphase conditions.

ACKNOWLEDGEMENT

The work of two of the authors(M. Kitahara and J.D. Achenbach) was carried out in the course of Japan-US cooperative research project with Japan Society for the Promotion of Science and the US National Science Foundation.

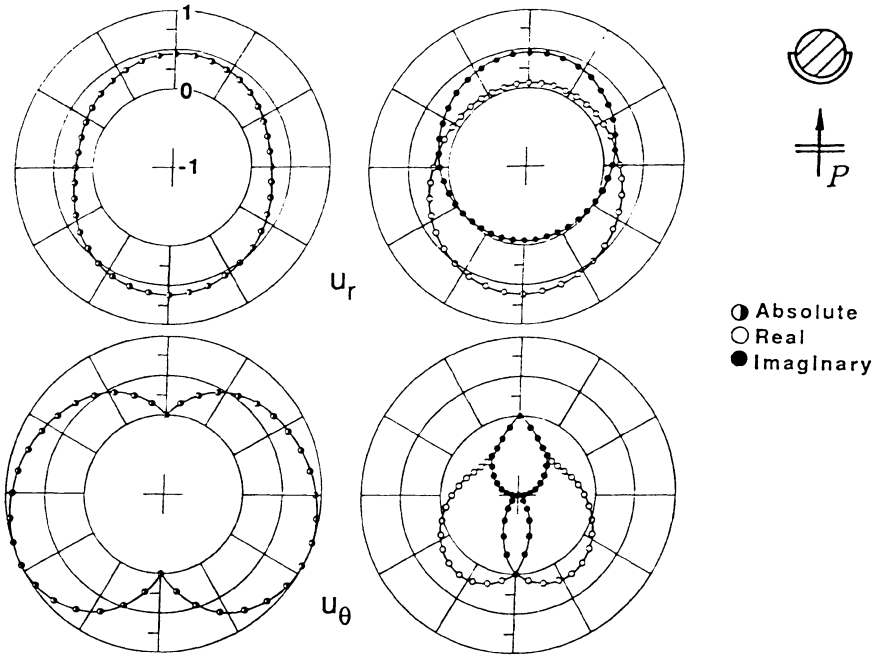

Fig.6 Radiation pattern for the case of crack at insonified side.

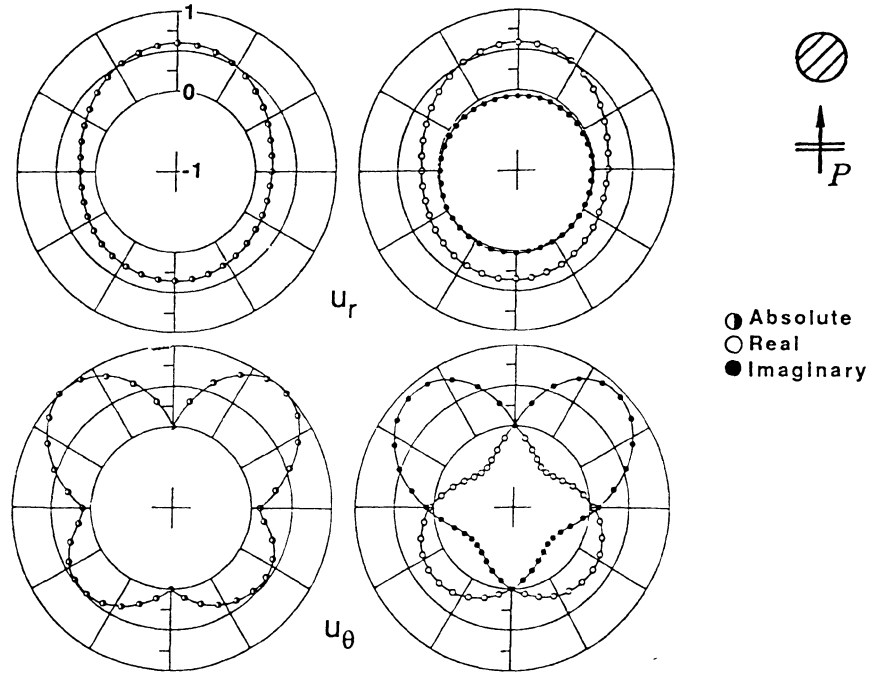

Fig.7 Radiation pattern for the case of perfect bonding.

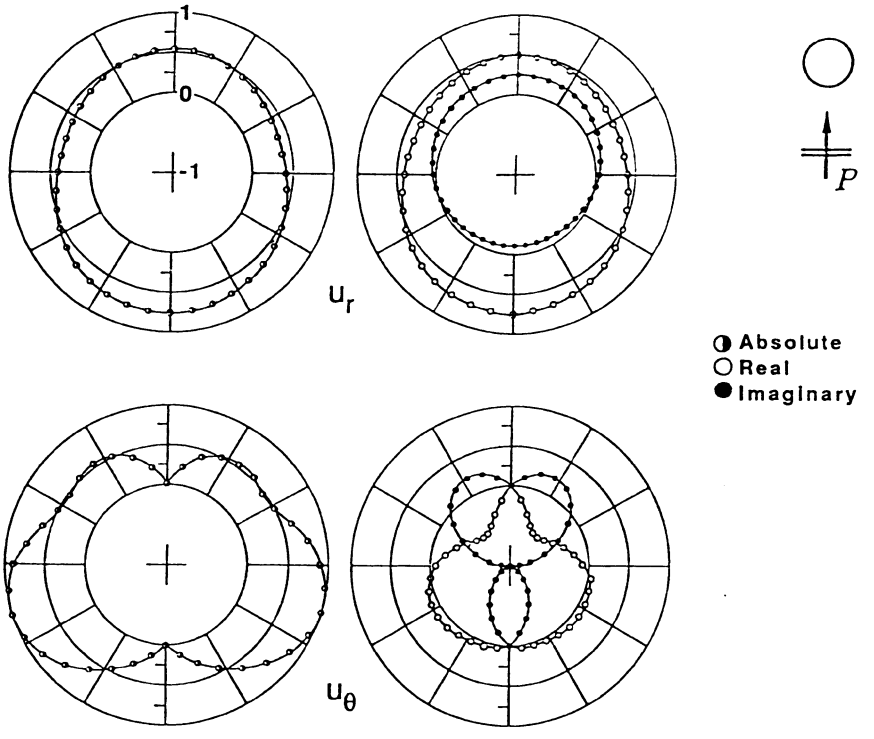

Fig.8 Radiation pattern for the case of cavity.

REFERENCES

1. M. Kitahara, K. Nakagawa and J.D. Achenbach, Backscatter from a spherical inclusion with compliant interphase characteristics, in Review of Progress in Quantitative NDE, Vol.8A, ed. by Thompson, D.O. and Chimenti, D.E., Plenum Press, New York, pp.47-54, 1989.
2. J.M. Baik and R.B. Thompson, The elastic compliance of imperfect interfaces: review and relationship to ultrasonic scattering, in Review of Progress in Quantitative NDE, Vol.4A, ed. by Thompson, D.O. and Chimenti, D.E., Plenum Press, New York, pp.133-144, 1985.
3. P.A. Martin, Thin interface layers: adhesives, approximations and analysis, IUTAM Symposium on Elastic Wave Propagation and NDE, Boulder, Colorado, July 30-August 3, 1989(Proceedings will be published by Elsevier).
4. M. Kitahara, K. Nakagawa and J.D. Achenbach, Boundary integral equation method for elastodynamic scattering by a compact inhomogeneity, Computational Mechanics, 1989(in press).